RESEARCH ARTICLE | FEBRUARY 06 2023

Kinetic theory of parametric decay instabilities near the upper hybrid resonance in plasmas

Jiangyue Han ; Zhe Gao ; S. K. Hansen

Physics of Plasmas 30, 022104 (2023)
https://doi.org/10.1063/5.0115517

Physics of Plasmas ARTICLE scitation.org/journal/php

Kinetic theory of parametric decay instabilities near the upper hybrid resonance in plasmas

Cite as: Phys. Plasmas **30**, 022104 (2023); doi: 10.1063/5.0115517
Submitted: 27 July 2022 · Accepted: 17 January 2023 ·
Published Online: 6 February 2023

Jiangyue Han,[1] Zhe Gao,[1,a)] and S. K. Hansen[2]

AFFILIATIONS

[1]Department of Engineering Physics, Tsinghua University, Beijing 100084, China
[2]Plasma Science and Fusion Center, Massachusetts Institute of Technology, Cambridge, Massachusetts 02139, USA

[a)]Author to whom correspondence should be addressed: gaozhe@tsinghua.edu.cn

ABSTRACT

Parametric decay instabilities (PDIs) near the upper hybrid resonance layer are studied with a 1D framework. In a uniform plasma, the kinetic nonlinear dispersion relation of PDI is numerically calculated for parameters corresponding to electron cyclotron heating experiments at the ASDEX-U tokamak, in which O-mode radiation was converted to X-mode radiation by reflection from the high-field sidewall. The forward scattering processes driven by X-mode and linearly converted electron Bernstein waves (EBWs) are investigated and found to lead to a primary PDI where the pump waves decay into lower hybrid waves and sideband EBWs. A frequency shift of 930 MHz is obtained for the sideband EBWs in the primary PDIs. Subsequently, the sideband EBWs can decay into a low-frequency ion Bernstein quasi-mode (IBQM) and a secondary EBW, where the dominant forward scattering channel is the first-order IBQM with a frequency close to twice the ion cyclotron frequency. The decay channels obtained by numerical calculation can explain the characteristics of the signal observed in ASDEX-U experiments. The threshold of the pump electric field strength required to excite the primary PDI in the presence of plasma inhomogeneity is also estimated.

I. INTRODUCTION

Parametric decay instability (PDI) in plasma is a common nonlinear process. When the intensity of a pump wave exceeds a nonlinear threshold, it decays into daughter waves whose frequencies and wave vectors satisfy the selection rule. PDI has been extensively studied in ionospheric plasmas,[1] inertial confinement fusion plasmas,[2] and magnetic confinement fusion plasmas.[3,4]

Since the 1970s, various microwave heating and current drive methods have been introduced into magnetically confined plasma experiments, utilizing lower hybrid waves (LHWs),[5] electron cyclotron waves,[6] and ion cyclotron waves.[7] PDI occurs when the injected power exceeds a certain threshold, and its relationship with the input power shows obvious nonlinear characteristics,[3,8] which have been confirmed by a large number of experimental observations. PDI will transfer the energy of the injected pump wave to the daughter waves, resulting in a modification of the efficiency of heating[9] and current drive,[10] and even damage to diagnostic components.[11] On the other hand, PDI enables the coupling of waves with frequencies of different orders of magnitude, providing a possible explanation for the unexpected generation of fast ions[12,13] or suprathermal electrons[14,15] observed in experiments. Future magnetic confinement fusion devices require higher-power microwave injection, so PDI will be more likely to occur.

A pump wave with a frequency on the order of electron cyclotron frequency can excite low-frequency oscillations more easily near the upper hybrid resonance (UHR) layer due to the field enhancement effect[16] in the resonance region. The PDI near the UHR layer was first observed by Hiroe and Ikegami.[17] In that experiment, lower hybrid modes were excited by a strongly nonlinear process. Later, in the L-3 linear device,[9,18] the FM-1 spherator,[19] and the TM-3 tokamak,[20] it was observed that electron cyclotron waves parametrically decay into electron Bernstein waves (EBWs), LHWs, and ion-acoustic waves. Additionally, it was found that the plasma was heated significantly when the pump power exceeded the threshold but without confinement degradation. In electron cyclotron resonance heating experiments with higher input power, a common mechanism is understood to be that the pump wave excites an EBW first, and then the EBW drives the PDI. Related spectra have been observed in Versator II,[8] FT-1,[21] W7-AS,[22] and MAST.[23]

The PDI theory near the UHR layer has been studied by a number of researchers. Porkolab[24] developed a theory of PDI based on fluid equations and systematically studied the possibility and impact of

parametric instability during ECRH experiments in the MTX tokamak.[4] Stefan *et al.*[25] and Cohen[26] derived a more general dispersion relation for parametric instabilities in magnetized plasmas, taking into account finite pump wave numbers. Liu and Tripathi[27] established a kinetic theory within the guiding center formalism to describe the PDIs and studied decay channels of electron cyclotron waves in detail. Then, the kinetic theory was applied to study the PDI of an X-mode wave into a high-frequency EBW and a low-frequency ion Bernstein wave (IBW) in ionospheric modification experiments.[28] More recently, Dodin[29] and Arefiev[30] investigated the same process using a variational approach along with the cold plasma dispersion relation and extended it to strong pump strength regimes.

Although the case we are concerned about in this paper is PDI near the UHR layer, it must be noted that this is not the only case in ECRH experiments. Another important type of PDI occurs in the region of a magnetic island when auxiliary electron heating is used to suppress the development of neoclassical tearing modes,[12,31] where a low-threshold PDI theory in the presence of a nonmonotonic density profile has been well-established by Gusakov and Popov.[13,32]

Collective Thomson scattering (CTS) diagnostics were applied to detect PDI signals during ECRH experiments in some tokamaks, including FTU,[33] TEXTOR,[34] and ASDEX-U.[35] The unprecedented MHz-level frequency resolution of the fast acquisition systems[36] used for CTS measurements made it possible to observe parametric decay into channels besides the one involving EBWs and LHWs as daughter waves.

Recently, Hansen *et al.*[37,38] reported experimental observations of ASDEX-U in which spectrum measured by CTS diagnostics can be attributed to PDIs occurring near UHR layer. In the experiments, O-mode ($f_0 \approx 105\,\mathrm{GHz}$) radiation is injected from the low-field side (LFS) and then reflected off the inner wall on the high-field side (HFS). This reflection process converts a fraction of the O-mode radiation to X-mode radiation. Due to the field enhancement effect, when the X-mode radiation propagates near the UHR layer, its amplitude is large enough to excite an EBW parametrically, besides by linear mode conversion. However, the frequency shift estimated by the simple PDI theory used in Refs. 37 and 38 is far from the experimental value due to the use of the dipole approximation. Associated particle-in-cell (PIC) simulations[39] produced frequency shifts closer to the experimental observations but required modifications of the electron density and magnetic field profiles to produce self-consistent results. Additionally, the secondary PDI driven by the sideband EBW, which has a frequency gap of $50\,\mathrm{MHz}(\sim 2\omega_{ci})$, would require PIC simulations of excessive length to be studied. In this paper, we adopt a more general theory to calculate the frequency shift of the primary PDI and explain the frequency gap of the secondary cascade PDI.

The paper is organized as follows. Section II describes the kinetic PDI theory concerning the waves driven near the UHR layer, where the nonlinear dispersion equations are derived in the electrostatic and electromagnetic framework. Section III presents the results of numerical calculations and discusses their interpretation. Finally, Sec. IV presents our discussion and conclusion.

II. KINETIC THEORY OF PARAMETRIC INSTABILITIES

In this section, we give a brief introduction to the theoretical model. The general formalism of kinetic theory was established by Liu and Tripathi[27] to study PDI in magnetized plasmas in 1986. The nonlinear dispersion relation, although only containing quasi-linear (QL) terms, is so costly to numerically solve that it is rarely used in related studies. Until recently, to explain the spectral gap problem in lower hybrid current drive, Liu *et al.*[40,41] extended the kinetic theory by including the higher-order nonlinearities of the parametric process. The results show that the QL method (i.e., the original model in Ref. 27) is sufficient to describe the PDI process when resonant decay occurs. However, when the low-frequency modes are heavily damped quasi-modes, nonlinear correction of the sidebands is essential, requiring the use of the QL-NL (quasi-linear low-frequency and nonlinear sidebands) method. Consider a pump wave $(\omega_0, \boldsymbol{k}_0)$ propagating in a magnetized plasma with a uniform static magnetic field $B_0\hat{\boldsymbol{e}}_z$, and decaying into a low-frequency mode $(\omega_s, \boldsymbol{k}_s)$ and two sidebands $(\omega_{1,2}, \boldsymbol{k}_{1,2})$. The frequencies and wave vectors satisfy the selection rules,

$$\omega_1 = \omega_0 - \omega_s, \quad \boldsymbol{k}_1 = \boldsymbol{k_0} - \boldsymbol{k}_s, \quad \omega_2 = \omega_0 + \omega_s, \quad \boldsymbol{k}_2 = \boldsymbol{k_0} + \boldsymbol{k}_s. \tag{1}$$

Next, we will calculate the nonlinear contributions to the dispersion relation within the electromagnetic and electrostatic framework, respectively (see Ref. 41 for a more detailed derivation).

Unlike the commonly used three-wave model, we retain the effects of the upshifted and downshifted sidebands at the same time and build a simple four–wave interaction model (actually two processes of three-wave interaction with upshifted/downshifted sidebands). This treatment is reasonable because the experimentally observed signal strengths of the upshifted and downshifted sidebands are on the same order of magnitude, especially for secondary peaks in the main sideband signal.[38] By ignoring the upshifted sideband, we can easily return to the nonlinear dispersion relation of the three-wave model, and the comparison of these two models will be shown in Sec. III. Furthermore, a vital approximation is to consider electron nonlinearity only since ion nonlinearity is negligible in most cases.[42]

A. Electromagnetic framework

The perturbative current density due to a single species can be obtained by integrating the distribution function multiplied by the velocity vector,

$$\boldsymbol{J}_j = -Sq\int_0^\infty d\mu \int_0^{2\pi} d\theta \int_{-\infty}^{\infty} dp_z \boldsymbol{v} f^j, \tag{2}$$

where $S=1$ for electrons and $S=-1$ for ions, and q is the particle charge. Substituting Eq. (2). into Maxwell's equations, the electromagnetic dispersion equation can be written as follows:

$$\boldsymbol{D}_j \cdot \boldsymbol{E}_j = -\frac{4\pi i}{\omega_j}\boldsymbol{J}_j^{NL}, \tag{3}$$

where $\boldsymbol{D}$ is the linear dielectric tensor

$$\boldsymbol{D}_j = \boldsymbol{\varepsilon}_j - \frac{c^2}{\omega_j^2}k_j^2\boldsymbol{I} + \frac{c^2}{\omega_j^2}\boldsymbol{k}_j\boldsymbol{k}_j, \tag{4}$$

and $\boldsymbol{\varepsilon}_j = \boldsymbol{I} + 4\pi i\boldsymbol{\sigma}_j^L/\omega_j$ is the linear permittivity tensor with $\boldsymbol{\sigma}_j^L$ being the linear conductivity tensor. The solution of $|\boldsymbol{D}_j(\omega, k)| = 0$ is the linear dispersion relation of wave j. The linear perturbative current density has been moved to the left-hand side of Eq. (3), while the

nonlinear perturbative current density $\boldsymbol{J}_j^{NL}$ is the integral with $f^j = f_j^{NL}$ in Eq. (2). For the QL method, we can organize the extra nonlinear current density in the following form:

$$\begin{aligned} \boldsymbol{J}_s^{NL} &= \boldsymbol{\sigma}_{s1}^{QL} \cdot \boldsymbol{E}_1 + \boldsymbol{\sigma}_{s2}^{QL} \cdot \boldsymbol{E}_2, \\ \boldsymbol{J}_1^{NL} &= \boldsymbol{\sigma}_1^{QL} \cdot \boldsymbol{E}_s, \\ \boldsymbol{J}_2^{NL} &= \boldsymbol{\sigma}_2^{QL} \cdot \boldsymbol{E}_s, \end{aligned} \tag{5}$$

where $\boldsymbol{\sigma}_{jk}^{QL}$ are quasi-linear conductivity tensors (see Eqs. (18)–(22) in Ref. 41 for full expressions). Then, Eq. (3) can be written as follows:

$$\begin{pmatrix} \boldsymbol{D}_s & \tilde{\boldsymbol{\sigma}}_{s1}^{QL} & \tilde{\boldsymbol{\sigma}}_{s2}^{QL} \\ \tilde{\boldsymbol{\sigma}}_1^{QL} & \boldsymbol{D}_1 & 0 \\ \tilde{\boldsymbol{\sigma}}_2^{QL} & 0 & \boldsymbol{D}_2 \end{pmatrix} \cdot \begin{pmatrix} \boldsymbol{E}_s \\ \boldsymbol{E}_1 \\ \boldsymbol{E}_2 \end{pmatrix} = 0, \tag{6}$$

where $\tilde{\sigma}_{jk} = (4\pi i/\omega_j)\sigma_{jk}$. The square matrix on the left hand side of Eq. (6) is the nonlinear dispersion matrix, which is a 9×9 matrix. By setting the determinant of nonlinear dispersion matrix equal to zero, we can then obtain the electromagnetic dispersion relation of resonant four-wave parametric processes,

$$\begin{vmatrix} \boldsymbol{D}_s & \tilde{\boldsymbol{\sigma}}_{s1}^{QL} & \tilde{\boldsymbol{\sigma}}_{s2}^{QL} \\ \tilde{\boldsymbol{\sigma}}_1^{QL} & \boldsymbol{D}_1 & 0 \\ \tilde{\boldsymbol{\sigma}}_2^{QL} & 0 & \boldsymbol{D}_2 \end{vmatrix} = 0. \tag{7}$$

For the QL-NL method, we retain higher order nonlinearity of the sidebands and represent the nonlinear current density as follows:

$$\begin{aligned} \boldsymbol{J}_s^{NL} &= \boldsymbol{\sigma}_{s1}^{QL} \cdot \boldsymbol{E}_1 + \boldsymbol{\sigma}_{s2}^{QL} \cdot \boldsymbol{E}_2, \\ \boldsymbol{J}_1^{NL} &= \boldsymbol{\sigma}_1^{QL} \cdot \boldsymbol{E}_s + \boldsymbol{\sigma}_{1s}^{NL} \cdot \boldsymbol{E}_1, \\ \boldsymbol{J}_2^{NL} &= \boldsymbol{\sigma}_2^{QL} \cdot \boldsymbol{E}_s + \boldsymbol{\sigma}_{2s}^{NL} \cdot \boldsymbol{E}_2. \end{aligned} \tag{8}$$

Similarly, the electromagnetic dispersion relation for the QL-NL method, which is necessary to study quasi-mode decay, is

$$\begin{vmatrix} \boldsymbol{D}_s & \tilde{\boldsymbol{\sigma}}_{s1}^{QL} & \tilde{\boldsymbol{\sigma}}_{s2}^{QL} \\ \tilde{\boldsymbol{\sigma}}_1^{QL} & \boldsymbol{D}_1 + \tilde{\boldsymbol{\sigma}}_{1s}^{NL} & 0 \\ \tilde{\boldsymbol{\sigma}}_2^{QL} & 0 & \boldsymbol{D}_2 + \tilde{\boldsymbol{\sigma}}_{2s}^{NL} \end{vmatrix} = 0. \tag{9}$$

B. Electrostatic framework

The kinetic theory of PDI in the electromagnetic framework is complete. However, its formulas are complicated, and the numerical calculations are time-consuming. In some cases, the waves involved (such as EBWs and IBWs) can be approximately described by electrostatic linear dispersion relations. Then, the nonlinear dispersion relation can also be simplified within the electrostatic framework.

The electron density perturbation can be obtained by integrating the distribution function directly,

$$n_j = \int_0^\infty d\mu \int_0^{2\pi} d\theta \int_{-\infty}^\infty dp_z f^j. \tag{10}$$

By substituting Eq. (10) into Poisson's equation, the electrostatic nonlinear dispersion equation can be written as follows:

$$\varepsilon_j^L \phi_j = -\frac{4\pi e}{{k_j}^2} n_j^{NL}, \tag{11}$$

where $\varepsilon_j^L = 1 + \chi_j$ is the linear permittivity, χ_j is the susceptibility, and e is the elementary charge. For the QL method, we organize the nonlinear density perturbation as follows:

$$\begin{aligned} n_s^{NL} &= \frac{{k_s}^2}{4\pi e} \chi_{s1}^{QL} \phi_1 + \frac{{k_s}^2}{4\pi e} \chi_{s2}^{QL} \phi_2, \\ n_1^{NL} &= \frac{{k_1}^2}{4\pi e} \chi_1^{QL} \phi_s, \\ n_2^{NL} &= \frac{{k_2}^2}{4\pi e} \chi_2^{QL} \phi_s. \end{aligned} \tag{12}$$

Then, Eq. (11) can be written as follows:

$$\begin{pmatrix} \varepsilon_s^L & \chi_{s1}^{QL} & \chi_{s2}^{QL} \\ \chi_1^{QL} & \varepsilon_1^L & 0 \\ \chi_2^{QL} & 0 & \varepsilon_2^L \end{pmatrix} \cdot \begin{pmatrix} \phi_s \\ \phi_1 \\ \phi_2 \end{pmatrix} = 0. \tag{13}$$

Thus, within the electrostatic framework, the nonlinear dispersion matrix is a 3×3 matrix. The electrostatic dispersion relation of resonant four-wave parametric processes is

$$\begin{vmatrix} \varepsilon_s^L & \chi_{s1}^{QL} & \chi_{s2}^{QL} \\ \chi_1^{QL} & \varepsilon_1^L & 0 \\ \chi_2^{QL} & 0 & \varepsilon_2^L \end{vmatrix} = 0. \tag{14}$$

It is worth mentioning that Eq. (14) can be reduced to the usual form

$$\varepsilon_s^L = \frac{\mu_1}{\varepsilon_1^L} + \frac{\mu_2}{\varepsilon_2^L}, \tag{15}$$

where $\mu_1 = \chi_{s1}^{QL}\chi_1^{QL}, \mu_2 = \chi_{s2}^{QL}\chi_2^{QL}$ are coupling coefficients.

Similarly, the electrostatic dispersion relation for the QL-NL method, which is necessary to study quasi-mode decay, is

$$\begin{vmatrix} \varepsilon_s^L & \chi_{s1}^{QL} & \chi_{s2}^{QL} \\ \chi_1^{QL} & \varepsilon_1^L + \chi_{1s}^{NL} & 0 \\ \chi_2^{QL} & 0 & \varepsilon_2^L + \chi_{2s}^{NL} \end{vmatrix} = 0. \tag{16}$$

The electrostatic dispersion relation in Eq. (16) takes 1–2 orders of magnitude less solution time than the electromagnetic dispersion relation in Eq. (9).

III. NUMERICAL CALCULATIONS

The nonlinear dispersion relation derived in Sec. II can be solved numerically. Parameters characteristic of the ASDEX-U experiment discussed in Ref. 38 are considered: $B_s = 3.34\text{T}$, $n_e = 3.09 \times 10^{19}\ \text{m}^{-3}$, $f_0 = 105\ \text{GHz}$, $T_e = T_i = 650\ \text{eV}$, $Z_i = 1$, $m_i/m_e = 2 \times 1836$. Under such parameters, some characteristic frequencies are $f_{ci} \approx 25\ \text{MHz}$, $f_{ce} \approx 93\ \text{GHz}$, $f_{pe} \approx 50\ \text{GHz}$, $f_{LH} \approx 726\ \text{MHz}$, and $f_{UH} \approx 105.8\ \text{GHz}$.

We assume that the pump wave propagates perpendicular to the background magnetic field $\boldsymbol{k}_0 = k_0 \boldsymbol{e}_x$, where the background magnetic field is in the z direction $\boldsymbol{B}_0 = B_s \boldsymbol{e}_z$. From the linear dispersion relation $|\boldsymbol{D}_0(\omega, k)| = 0$, we have $n_0 = k_0 c/\omega_0 = 4.64$ and the electric field vector of the X-mode pump wave is $\boldsymbol{E}_0 = (0.9992, -0.0412i, 0.0002)E_0$. The polarization of the pump wave shows obvious longitudinal wave characteristics.

We present our calculation results in a model geometry of 1D forward scattering since it produces results consistent with the experimental observations. In this model, we have $\omega_s \ll \omega_0 \sim \omega_{1,2}, k_s \ll k_0 \sim k_{1,2}$. For the given parameters, we set a perpendicular wavenumber $n_\perp = k_\perp c/\omega_0$ of the daughter wave and then calculate the complex frequency $\omega = \omega_r + i\gamma$ that satisfies the nonlinear dispersion relation. Specifically, we use the pattern search method to find the maximum value of the condition number of the nonlinear dispersion matrix, which is mathematically equivalent to the dispersion equations in Sec. II but more efficient. By scanning the wave vectors, we can obtain the complete dispersion curves. On dispersion curves, the values of $n_\perp$ with positive linear growth rate $\gamma > 0$ are PDI unstable. The wavenumber and real frequency corresponding to the maximum positive growth rate can help us identify the type of daughter wave.

A. Resonant decay

In our model, all waves propagate approximately perpendicular to the background magnetic field. Pump waves and sideband waves have small k_z satisfying $k_{0z}v_e/\omega_0 \ll 1, k_{1z}v_e/\omega_1 \ll 1, k_{2z}v_e/\omega_2 \ll 1$ due to their high frequencies. For the case of resonant decay, Landau damping of the low-frequency wave can be neglected, so $k_{sz}v_e/\omega_s \ll 1$ is also satisfied.

In our calculations, the pump waves included are the incoming X-mode wave and the linearly converted EBW (abbreviated to EBW-L) since PDI occurs near the UHR layer and linear mode conversion cannot be ignored. We use the QL-method within the electromagnetic framework of Eq. (7) to study resonant decay because the X-mode wave is electromagnetic and cannot be obtained from an electrostatic dispersion relation. In order to compare the effects of different pump waves on parametric excitation, the case of an EBW-L pump is also calculated by the QL-method within the electromagnetic framework.

First, we calculate dispersion curves by the four-wave model (including the upshifted sideband) and the three-wave model (neglecting the upshifted sideband) for the same parameters, as shown in Fig. 1. The results of the two methods are essentially identical, indicating that in this case the upshifted sideband is not important. As with most parametric processes, the upshifted sideband is off-resonant.

The calculation results at different pump field strengths are shown in Fig. 2. The real frequency of the solutions with positive

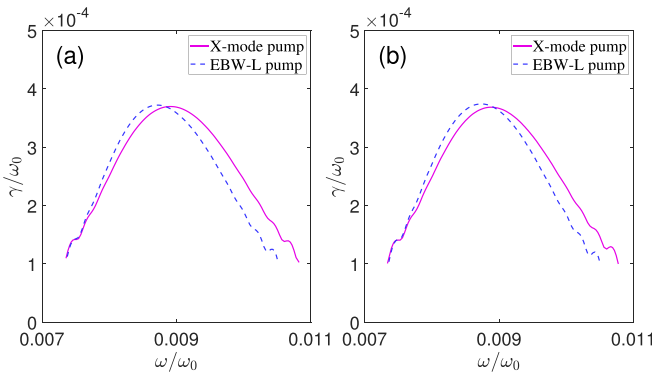

FIG. 1. The linear growth rate of the resonant decay at $E_0 = 3$MeV/m (a) including the upshifted sideband and (b) neglecting the upshifted sideband.

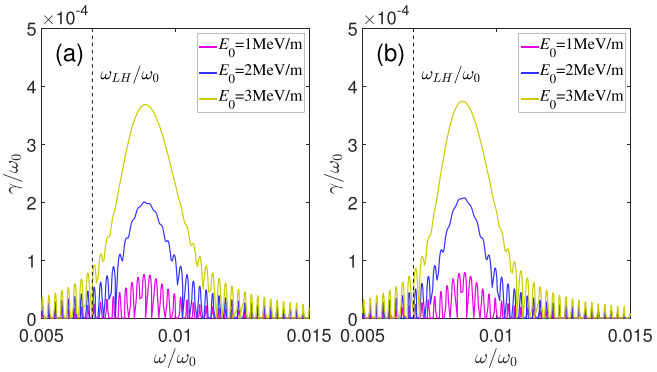

FIG. 2. The linear growth rate of the resonant decay neglecting the upshifted sideband: (a) X-mode pump, $n_{0\perp} = 4.64$ and (b) EBW-L pump, $n_{0\perp} = 4.82$.

growth rates $\gamma > 0$ ranges from 500 to 1500 MHz. Outside of this range, the linear growth rate is small and can be ignored. When the pump intensity is small, the growth rate curve has a multi-peaked structure, because the daughter wave is a high-order IBW, and its linear kinetic dispersion curve is separated by integer multiples of ω_{ci}. This is why the real frequency gap between adjacent peaks is approximately ω_{ci}. At the same pump intensity, the linear growth rates of PDIs driven by X-mode pump and EBW-L pump waves are almost identical, mainly because the two pump waves are very similar near the UHR layer. As the pump intensity increases, these small peaks broaden and evolve into a smooth curve as illustrated in Figs. 2(a) and 2(b).

The low-frequency wave of the shown decay channel was identified as an LHW in previous work.[38] In our calculation, γ reaches its maximum at $\omega_r/\omega_0 \sim 0.0089$, so the real frequency of the daughter wave estimated by our kinetic theory is 930 MHz, which is close to the experimentally observed frequency from Ref. 37. This PDI process with a considerable frequency gap is easiest to observe, and we call it the primary PDI.

Next, we discuss the pump threshold required for resonant decay. In the resonant decay case, the upshifted sideband is non-resonant so a classic three-wave convective model is adequate. Moreover, since we only consider forward scattering, the wavenumber mismatch caused by the finite pump extent can be ignored. Here, we mainly estimate the convective amplification related to plasma inhomogeneity by the Piliya–Rosenbluth criterion,[43,44]

$$A = \frac{\gamma^2}{|v_{gs}v_{g1}K'|} > 1, \tag{17}$$

where A is the convective amplification factor, v_{gs} is the group velocity of the low-frequency wave, v_{g1} is the group velocity of the downshifted sideband wave, and $K' = \partial(k_{0x} - k_{sx} - k_{1x})/\partial x$. The x direction is the propagation direction of the waves. In this direction, the local density gradient is taken to be $dn_e/dx = 1 \times 10^{19}\ \mathrm{m}^{-3}/\mathrm{m}$, the local magnetic field gradient is taken to be $dB_s/dx = -3\ \mathrm{T}/\mathrm{m}$, and the local temperature gradient is taken to be $dT_e/dx = dT_i/dx = 2\ \mathrm{keV}/\mathrm{m}$, based on the experimental gradients near the UHR in the ASDEX-U experiment from Ref. 37. Linear growth rates and amplification factor at different pump intensities are shown in Fig. 3.

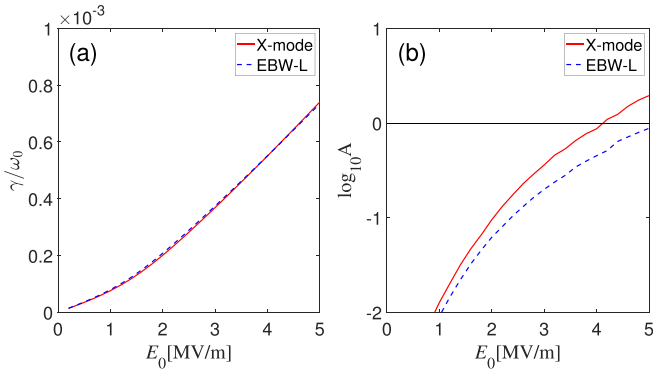

FIG. 3. (a) Maximum linear growth rate and (b) amplification factor vs pump field strength.

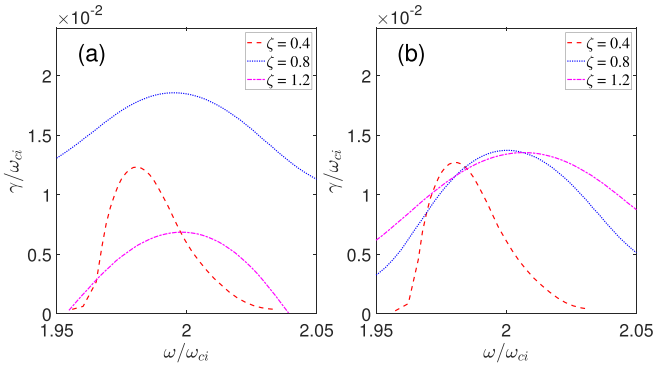

FIG. 4. The linear growth rate of the quasi-mode decay at $\omega_s \sim 2\omega_{ci}$ (a) including the upshifted sideband and (b) neglecting the upshifted sideband.

Figure 3(a) shows that X-mode and EBW-L pump waves have almost identical maximum linear growth rates. The X-mode pump wave has a lower threshold as illustrated in Fig. 3(b). This is because its low-frequency LHW has a larger wave vector, i.e., a smaller group velocity. From this point of view, it is easier for the X-mode wave to directly excite the LHW, and the field strength of the X-mode wave is also greater. The threshold from Fig. 3(b) is about 4 MV/m, which is consistent with the amplitude of approximately 4 MV/m observed in PIC simulations of ASDEX-U-like conditions at pump wave intensities just above the PDI threshold.[39]

B. Quasi-mode decay

In addition to the primary PDI, experimental observations[38] of discrete peaks in the sideband signals indicate the occurrence of a secondary PDI. In this section, we study the decay channel involving low-frequency daughter with frequencies on the order of ω_{ci}. Quasi-electrostatic waves propagating perpendicular to the magnetic field and possessing frequencies on the order of the ion cyclotron frequency are IBWs. For $k_{s\perp}v_\perp/\omega_{ci} \ll 1$, the frequency of the Nth-order IBW is approximately $(N+1)\omega_{ci}$.[45]

We initially investigated the case of resonant decay to IBWs by ignoring Landau damping. However, the results showed that there is no decay channel if k_{sz} is too small. Therefore, we remove the restriction $k_{sz}v_e/\omega_s \ll 1$ and consider quasi-mode decay case. The pump wave of the quasi-mode decay is assumed to be the sideband wave of the primary PDI, which is an EBW. The secondary daughter waves we are interested in will be those with frequencies in the ion cyclotron frequency range, such as IBWs. The secondary pump, sideband, and low-frequency daughter waves propagate perpendicular to the background magnetic field and can be described by the linear electrostatic dispersion relation. In this part, the electrostatic nonlinear dispersion relation of Eq. (16) will be applied. The parameters used in the calculations are $f_0' = 104\text{GHz}$, $e\phi_0'/T_e = 0.05$. Other parameters are the same as for the primary PDI.

The growth rate curves calculated by the four-wave model (including the upshifted sideband) and the three-wave model (neglecting the upshifted sideband) are shown in Fig. 4. The variable parameter ζ is defined as $\zeta = k_{sz}v_e/2\omega_{ci}$. When $\zeta \sim 1$, the low-frequency wave would suffer strong electron Landau damping. For $\zeta < 0.5$, the dispersion curves of the two models are essentially identical. However, for $\zeta > 0.5$, there is a large deviation between the calculation results of the two models. The growth rate obtained by the four-wave model reaches its maximum at $\zeta \sim 0.8$ and decays to 0 around $\zeta \sim 1.4$. By contrast, the growth rate obtained by the three-wave model remains approximately unchanged after $\zeta = 0.8$. Through this comparison, we found that it is necessary to take the coupling to the upshifted sideband wave into account for the case of quasi-mode decay.

We change k_{sz} continuously and identify the maximum growth rate at different k_{sz}. The results are shown in Fig. 5. For forward scattering, the growth rates are very small for $k_{sz}v_e/\omega_s \ll 1$ and $k_{sz}v_e/\omega_s \gg 1$. When $k_{sz}v_e/\omega_s \sim 1$, the electron Landau damping is significant and the growth rates are largest. So strictly speaking, the low-frequency waves should be called IBQMs. The first order IBQM $(\omega_s \sim 2\omega_{ci} \sim 50\text{MHz})$ has the largest growth rate. For the cases with higher order $(N > 3)$, the growth rate decreases rapidly as the order increases.

Through the above analysis, the secondary PDI is identified as a process in which the primary EBWs decay into IBQMs and secondary EBWs.

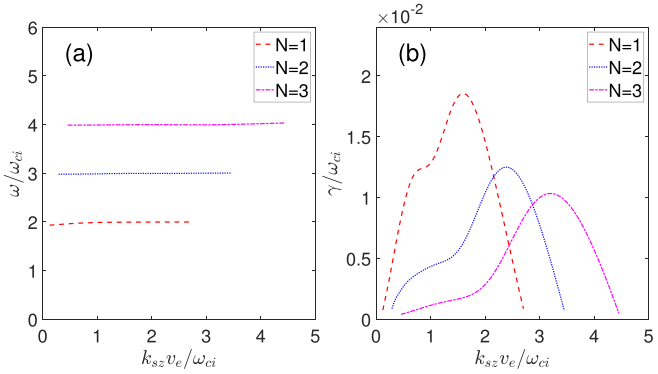

FIG. 5. Solution of the nonlinear dispersion relation with different k_{sz} for quasi-mode decay including the upshifted sideband: (a) Real frequency and (b) maximum growth rate.

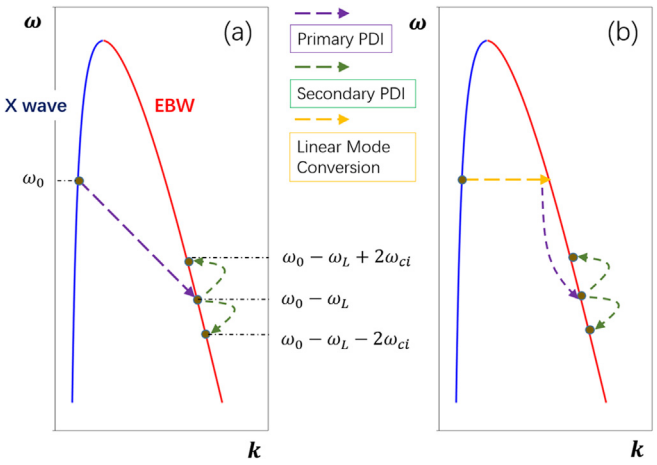

FIG. 6. Schematic diagram of the PDI process near the UHR layer: (a) X-mode pump and (b) EBW-L pump.

IV. DISCUSSION AND CONCLUSION

In this paper, we have applied a kinetic theory to study PDI processes near the UHR layer. Guided by experimental observations, we studied two parametric processes, referred to as the primary and secondary PDI, respectively. We first studied the influence of the upshifted sideband wave, and the results showed that for the primary PDI, the upshifted sideband wave can be ignored. For the secondary PDI, the calculation results of the three-wave model and the four-wave model are significantly different, so the upshifted sideband wave cannot be ignored in that case. Next, by solving the nonlinear dispersion relation numerically, we confirmed the primary and secondary decay channels and estimated the electric field threshold of the primary PDI. As shown in Fig. 6, X-mode waves and EBWs generated by linear mode conversion can decay into LHWs and sideband EBWs. Sideband EBWs can decay further into IBQMs and secondary sideband EBWs. Theoretically, the EBW-L can also decay into IBQMs and sideband EBWs. However, signals with frequencies close to the pump frequency are experimentally filtered by a notch filter; therefore, this process is not shown in Fig. 6.

The obtained results can provide an explanation to the observations from ASDEX-U. It should be pointed out that both linearly mode converted EBWs and parametrically excited EBWs will be completely absorbed at the electron cyclotron resonance layer and will not propagate to the low-field side. In the experiments, the signal is only increased by around two orders of magnitude compared with the background level. This indicates that the process leading to the generation of the O-mode waves reaching the radiometer on the low-field side only involves a small fraction of the total beam power. In conclusion, the O-mode waves observed by the radiometer on the low-field side are most likely caused by scattering of the injected O-mode wave by the low-frequency daughter waves generated by PDIs. For the primary PDI, the real frequency of the low-frequency daughter wave with the maximum growth rate is 930 MHz, while the value of the frequency shift between the X-mode pump wave and the primary sideband signal is approximately 900 MHz. By comparison, the cold lower hybrid frequency around the UHR layer is 726 MHz, underestimating the experimental frequency shift, while the dipole PDI model[37] predicts a frequency shift of 1040 MHz, overestimating the experimental frequency shift. The pump wave electric field threshold is estimated to be 4 MV/m. This value is consistent with the electric field amplitude of ∼4 MV/m found near the UHR by PIC simulations at pump wave intensity levels just above the PDI threshold[39] using ASDEX-U-like plasma and beam parameters, indicating that the Rosenbluth-Piliya PDI threshold is a reasonable estimate. This result additionally indicates that the primary PDI power threshold is similar to the one found experimentally in Ref. 37. For the secondary PDI, our results show that the first-order ion Bernstein quasi-mode with a frequency near twice the ion cyclotron frequency is the dominant decay channel, which explains the frequency shift of approximately 50 MHz between the secondary peaks. In the experimental observations, the primary downshifted signals are obviously stronger than the primary upshifted signals. Unlike the asymmetry in the primary PDI, the amplitudes of the secondary peaks are quite symmetrical (relative to the center frequency of the primary sideband signal), which also indicates that the upshifted sideband component of the secondary PDI plays an important role.

There are still issues that require further study. When the X-mode wave power reaching the UHR layer in ASDEX-U was increased further, additional small peaks were observed between the secondary peaks. While the PDI models investigated in this paper provide potential explanations of these peaks, e.g., in terms of PDIs involving second-order IBWs as the low-frequency daughter waves, a detailed investigation of the cascade decay is left for future work. Other problems include the estimation of the PDI threshold of quasi-mode decay and saturation levels, which will require intensive theoretical and numerical studies.

ACKNOWLEDGMENTS

This work was supported by NSFC under Grant Nos. 11875177 and 11827810, and IAEA CRP F13019 with Research Contract No. 22733. One of the authors (S. K. Hansen) acknowledges support by an Internationalisation Fellowship (No. CF19-0738) from the Carlsberg Foundation.

AUTHOR DECLARATIONS

Conflict of Interest

The authors have no conflicts to disclose.

Author Contributions

Jiangyue Han: Data curation (equal); Investigation (equal); Software (equal); Writing – original draft (equal). **Zhe Gao:** Conceptualization (equal); Validation (equal); Writing – review & editing (equal). **Søren Kjer Hansen:** Validation (equal); Writing – review & editing (equal).

DATA AVAILABILITY

The data that support the findings of this study are available within the article.

REFERENCES

[1]A. Y. Wong and R. J. Taylor, "Parametric excitation in the ionosphere," Phys. Rev. Lett. **27**, 644–647 (1971).

[2]D. H. Froula, B. Yaakobi, S. X. Hu, P. Y. Chang, R. S. Craxton, D. H. Edgell, R. Follett, D. T. Michel, J. F. Myatt, W. Seka, R. W. Short, A. Solodov, and C. Stoeckl, "Saturation of the two-plasmon decay instability in long-scale-length plasmas relevant to direct-drive inertial confinement fusion," Phys. Rev. Lett. **108**, 165003 (2012).
[3]M. Porkolab, S. Bernabei, W. M. Hooke, R. W. Motley, and T. Nagashima, "Observation of parametric instabilities in lower-hybrid radio-frequency heating of tokamaks," Phys. Rev. Lett. **38**, 230–233 (1977).
[4]M. Porkolab and B. I. Cohen, "Parametric instabilities associated with intense electron cyclotron heating in the MTX tokamak," Nucl. Fusion **28**, 239–254 (1988).
[5]M. Brambilla, "Slow-wave launching at the lower hybrid frequency using a phased waveguide array," Nucl. Fusion **16**, 47–54 (1976).
[6]V. Erckmann and U. Gasparino, "Electron cyclotron resonance heating and current drive in toroidal fusion plasmas," Plasma Phys. Controlled Fusion **36**, 1869–1962 (1994).
[7]F. W. Perkins, "Heating tokamaks via the ion-cyclotron and ion-ion hybrid resonances," Nucl. Fusion **17**, 1197–1224 (1977).
[8]F. S. McDermott, "Observation of the parametric decay instability during electron cyclotron resonance heating on the Versator II tokamak," Phys. Fluids **25**, 1488–1490 (1982).
[9]B. Grek and M. Porkolab, "Observation of plasma heating due to parametric instabilities at the upper hybrid and at the cyclotron harmonic frequencies," Phys. Rev. Lett. **30**, 836–839 (1973).
[10]Y. Takase, M. Porkolab, J. J. Schuss, R. L. Watterson, C. L. Fiore, R. E. Slusher, and C. M. Surko, "Observation of parametric instabilities in the lower-hybrid range of frequencies in the high-density tokamak," Phys. Fluids **28**, 983–994 (1985).
[11]S. K. Hansen, A. S. Jacobsen, M. Willensdorfer, S. K. Nielsen, J. Stober, K. Höfler, M. Maraschek, R. Fischer, and M. Dunne, "Microwave diagnostics damage by parametric decay instabilities during electron cyclotron resonance heating in ASDEX Upgrade," Plasma Phys. Controlled Fusion **63**, 95002 (2021).
[12]E. Westerhof, S. K. Nielsen, J. W. Oosterbeek, M. Salewski, M. R. D. Baar, W. A. Bongers, A. Burger, B. A. Hennen, S. B. Korsholm, F. Leipold, D. Moseev, M. Stejner, D. J. Thoen, and TEXOR Team, "Strong scattering of high power millimeter waves in tokamak plasmas with tearing modes," Phys. Rev. Lett. **103**, 125001 (2009).
[13]E. Z. Gusakov and A. Y. Popov, "Low threshold parametric decay backscattering instability in tokamak electron cyclotron resonance heating experiments," Phys. Rev. Lett. **105**, 115003 (2010).
[14]S. Depierreux, C. Neuville, C. Baccou, V. Tassin, M. Casanova, P. E. Masson-Laborde, N. Borisenko, A. Orekhov, A. Colaitis, A. Debayle, G. Duchateau, A. Heron, S. Huller, P. Loiseau, P. Nicolai, D. Pesme, C. Riconda, G. Tran, R. Bahr, J. Katz, C. Stoeckl, W. Seka, V. Tikhonchuk, and C. Labaune, "Experimental investigation of the collective Raman scattering of multiple laser beams in inhomogeneous plasmas," Phys. Rev. Lett. **117**, 235002 (2016).
[15]P. Michel, M. J. Rosenberg, W. Seka, A. A. Solodov, R. W. Short, T. Chapman, C. Goyon, N. Lemos, M. Hohenberger, J. D. Moody, S. P. Regan, and J. F. Myatt, "Theory and measurements of convective Raman side scatter in inertial confinement fusion experiments," Phys. Rev. E **99**, 33203 (2019).
[16]R. B. White and F. F. Chen, "Amplification and absorption of electromagnetic waves in overdense plasmas," Plasma Phys. **16**, 565–587 (1974).
[17]S. Hiroe and H. Ikegami, "Excitation of lower hybrid oscillations at upper hybrid resonance by microwaves," Phys. Rev. Lett. **19**, 1414–1416 (1967).
[18]M. Porkolab, "Parametric instabilities in a magnetic field and possible applications to heating of plasmas," Nucl. Fusion **12**, 329–340 (1972).
[19]M. Okabayashi, K. Chen, and M. Porkolab, "Experimental investigation of plasma heating by a high-frequency electric field near the electron cyclotron resonance in the FM-1 spherator," Phys. Rev. Lett. **31**, 1113–1116 (1973).
[20]V. V. Alikaev, G. A. Bobrovskii, M. M. Ofitserov, V. I. Poznyak, and K. A. Razumova, "Electron-cyclotron heating in the tokamak TM-3 installation," Sov. J. Exp. Theor. Phys. Lett. **15**, 27 (1972).
[21]D. G. Bulyginskii, "Nonlinear phenomena during electron cyclotron resonance heating in the FT-1 tokamak," Sov. J. Plasma Phys **12**, 77 (1986).
[22]H. P. Laqua, V. Erckmann, H. J. Hartfuß, and H. Laqua, "Resonant and nonresonant electron cyclotron heating at densities above the plasma cutoff by O-X-B mode conversion at the W7-AS stellarator," Phys. Rev. Lett. **78**, 3467–3470 (1997).
[23]V. Shevchenko, G. Cunningham, A. Gurchenko, E. Gusakov, B. Lloyd, M. O'Brien, A. Saveliev, A. Surkov, F. Volpe, and M. Walsh, "Development of electron Bernstein wave research in MAST," Fusion Sci. Technol. **52**, 202–215 (2017).
[24]M. Porkolab, "Parametric processes in magnetically confined CTR plasmas," Nucl. Fusion **18**, 367–413 (1978).
[25]V. Stefan, N. A. Krall, and J. B. McBride, "The nonlinear eikonal relation of a weakly inhomogeneous magnetized plasma upon the action of arbitrarily polarized finite wavelength electromagnetic waves," Phys. Fluids **30**, 3703–3712 (1987).
[26]B. I. Cohen, "Compact dispersion relations for parametric instabilities of electromagnetic waves in magnetized plasmas," Phys. Fluids **30**, 2676–2680 (1987).
[27]C. S. Liu and V. K. Tripathi, "Parametric instabilities in a magnetized plasma," Phys. Rep. **130**, 143–216 (1986).
[28]R. P. Sharma, A. Kumar, R. Kumar, and Y. K. Tripathi, "Excitation of electron Bernstein and ion Bernstein waves by extraordinary electromagnetic pump: Kinetic theory," Phys. Plasmas **1**, 522–527 (1994).
[29]I. Y. Dodin and A. V. Arefiev, "Parametric decay of plasma waves near the upper-hybrid resonance," Phys. Plasmas **24**, 32119 (2017).
[30]A. V. Arefiev, I. Y. Dodin, A. Köhn, E. J. D. Toit, E. Holzhauer, V. F. Shevchenko, and R. G. L. Vann, "Kinetic simulations of X-B and O-X-B mode conversion and its deterioration at high input power," Nucl. Fusion **57**, 116024 (2017).
[31]S. K. Nielsen, M. Salewski, E. Westerhof, W. Bongers, S. B. Korsholm, F. Leipold, J. W. Oosterbeek, D. Moseev, and M. Stejner, "Experimental characterization of anomalous strong scattering of mm-waves in TEXTOR plasmas with rotating islands," Plasma Phys. Controlled Fusion **55**, 115003 (2013).
[32]E. Z. Gusakov and A. Y. Popov, "Low threshold parametric decay instabilities in ECRH experiments at toroidal devices," Nucl. Fusion **51**, 73028 (2011).
[33]A. Bruschi, E. Alessi, W. Bin, O. D'Arcangelo, B. Baiocchi, F. Belli, G. Calabrò, I. Casiraghi, V. Cocilovo, L. Figini, C. Galperti, S. Garavaglia, G. Granucci, G. Grosso, S. B. Korsholm, M. Lontano, L. Lubyako, C. Mazzotta, V. Mellera, A. Moro, S. K. Nielsen, F. Orsitto, G. Ramogida, J. Rasmussen, D. Ricci, M. Stejner, and U. Tartari, "Observation of short time-scale spectral emissions at millimeter wavelengths with the new CTS diagnostic on the FTU tokamak," Nucl. Fusion **57**, 76004 (2017).
[34]S. K. Nielsen, M. Salewski, W. Bongers, S. B. Korsholm, F. Leipold, F. Meo, P. Michelsen, D. Moseev, J. W. Oosterbeek, M. Stejner, and E. Westerhof, "Modification of the collective Thomson scattering radiometer in the search for parametric decay on TEXTOR," Rev. Sci. Instrum. **83**, 113508 (2012).
[35]S. K. Nielsen, P. K. Michelsen, S. K. Hansen, S. B. Korsholm, F. Leipold, J. Rasmussen, M. Salewski, M. Schubert, M. Stejner, J. Stober, and D. Wagner, "Recent development of collective Thomson scattering for magnetically confined fusion plasmas," Phys. Scr. **92**, 24001 (2016).
[36]M. Stejner, S. Nielsen, A. S. Jacobsen, S. B. Korsholm, F. Leipold, F. Meo, P. K. Michelsen, D. Moseev, J. Rasmussen, M. Salewski, M. Schubert, J. Stober, D. H. Wagner, and ASDEX Upgrade, "Resolving the bulk ion region of millimeter-wave collective Thomson scattering spectra at ASDEX Upgrade," Rev. Sci. Instrum. **85**, 93504 (2014).
[37]S. K. Hansen, S. K. Nielsen, M. Salewski, M. Stejner, and J. Stober, "Parametric decay instability near the upper hybrid resonance in magnetically confined fusion plasmas," Plasma Phys. Controlled Fusion **59**, 105006 (2017).
[38]S. K. Hansen, S. K. Nielsen, J. Stober, J. Rasmussen, M. Salewski, and M. Stejner, "Power threshold and saturation of parametric decay instabilities near the upper hybrid resonance in plasmas," Phys. Plasmas **26**, 62102 (2019).
[39]M. G. Senstius, S. K. Nielsen, R. G. Vann, and S. K. Hansen, "Particle-in-cell simulations of parametric decay instabilities at the upper hybrid layer of fusion plasmas to determine their primary threshold," Plasma Phys. Controlled Fusion **62**, 25010 (2020).
[40]Z. Liu, Z. Gao, and A. Zhao, "Nonlinearity in parametric instabilities during the injection of lower hybrid waves into tokamak plasmas," Phys. Plasmas **26**, 42117 (2019).

[41]Z. Liu, Z. Gao, and A. Zhao, "Kinetic theory of parametric instabilities of lower hybrid waves in tokamaks in the electromagnetic framework," Phys. Plasmas **27**, 42503 (2020).
[42]V. K. Tripathi, C. S. Liu, and C. Grebogi, "Parametric decay of lower hybrid waves in a plasma: Effect of ion nonlinearity," Phys. Fluids **22**, 301–309 (1979).
[43]M. N. Rosenbluth, "Parametric instabilities in inhomogeneous media," Phys. Rev. Lett. **29**, 565 (1972).
[44]A. D. Piliya, "Nonstationary theory of decay instability in a weakly inhomogeneous plasma," Sov. Phys.-JETP **37**, 629–632 (1973).
[45]D. G. Swanson, *Plasma waves* (Elsevier, 2012).